

# Non-trivial role of interlayer cation states in iron-based superconductors

Daniel Guterding,<sup>1,\*</sup> Harald O. Jeschke,<sup>1</sup> I. I. Mazin,<sup>2</sup> J. K. Glasbrenner,<sup>3,†</sup> E. Bascones,<sup>4</sup> and Roser Valentí<sup>1</sup>

<sup>1</sup>*Institut für Theoretische Physik, Goethe-Universität Frankfurt,  
Max-von-Laue-Straße 1, 60438 Frankfurt am Main, Germany*

<sup>2</sup>*Code 6393, Naval Research Laboratory, Washington, DC 20375, USA*

<sup>3</sup>*National Research Council/Code 6393, Naval Research Laboratory, Washington, DC 20375, USA*

<sup>4</sup>*Instituto de Ciencia de Materiales de Madrid, ICMM-CSIC, Cantoblanco, 28049 Madrid, Spain*

Unconventional superconductivity in iron pnictides and chalcogenides has been suggested to be controlled by the interplay of low-energy antiferromagnetic spin fluctuations and the particular topology of the Fermi surface in these materials. Based on this premise, one would also expect the large class of isostructural and isoelectronic iron germanide compounds to be good superconductors. As a matter of fact, they, however, superconduct at very low temperatures or not at all. In this work we establish that superconductivity in iron germanides is suppressed by strong ferromagnetic tendencies, which surprisingly do not originate from changes in bond-angles or -distances with respect to iron pnictides and chalcogenides, but are due to changes in the electronic structure in a wide range of energies happening upon substitution of atom species (As by Ge and the corresponding spacer cations). Our results indicate that superconductivity in iron-based materials may not always be fully understood based on  $d$  or  $dp$  model Hamiltonians only.

*Introduction.*- After the initial discovery of high-temperature superconductivity in doped LaFeAsO [1], a large variety of other iron pnictides and chalcogenides have been shown to be superconductors [2], with some reports of the transition temperature  $T_c$  as high as 100 K [3]. On the other hand, isoelectronic and isostructural iron germanides are either non-superconducting [4–7] or possibly superconduct at very low temperatures [8, 9]. The currently most intensively debated material is YFe<sub>2</sub>Ge<sub>2</sub>, for which superconductivity below 2 K has been reported [9]. Its electronic structure is very similar to that of CaFe<sub>2</sub>As<sub>2</sub> in the collapsed tetragonal phase, but with significant hole-doping [9–11]. This led to speculation [9] about a connection between superconductivity in YFe<sub>2</sub>Ge<sub>2</sub> and the collapsed phase of the extremely hole-doped pnictide, KFe<sub>2</sub>As<sub>2</sub> [12–14]. Furthermore, Wang *et al.* [15] recently found YFe<sub>2</sub>Ge<sub>2</sub> to be close to a magnetic instability and X-ray absorption and photoemission experiments show evidence for strong spin-fluctuations [16] and moderate correlation effects [17] in this material.

It is generally agreed that magnetism plays an important role in superconductivity of Fe-based superconductors (FeBS) [2, 18–24]. It is therefore natural to ask whether the magnetic tendencies in iron germanides are fundamentally different from those in iron pnictides and chalcogenides [25] and why that is the case. In a first attempt to understand the lack of superconductivity in Fe germanides, a few authors investigated the electronic properties of the isoelectronic and isostructural materials MgFeGe and LiFeAs [26–28]. The former is a paramagnetic metal, while the latter is a superconductor. An important conclusion was that the dominant magnetic exchange interactions in MgFeGe are ferromagnetic, while those in LiFeAs are antiferromagnetic. The microscopic origin of this different behavior was, however, not further

explored.

In this Letter we show that (i) the presence of ferromagnetic tendencies is a general trait in iron germanides, which is detrimental for superconductivity, and that (ii) the ferromagnetic tendencies arise from the interaction of the cation spacer with the FeGe layer. In fact, the hole-doping or collapse of the  $c$ -axis in YFe<sub>2</sub>Ge<sub>2</sub> are not essential for this behavior, but the key is in substitution of As by Ge and the corresponding substitution of monovalent or divalent spacers by divalent or trivalent cations, respectively. This modifies the electronic bandstructure in a wide range of energies at and away from the Fermi level and creates ferromagnetic tendencies which suppress superconductivity. Hence, one can go from As to Se/Te, *i.e.*, right in the periodic table, and find further FeBS,

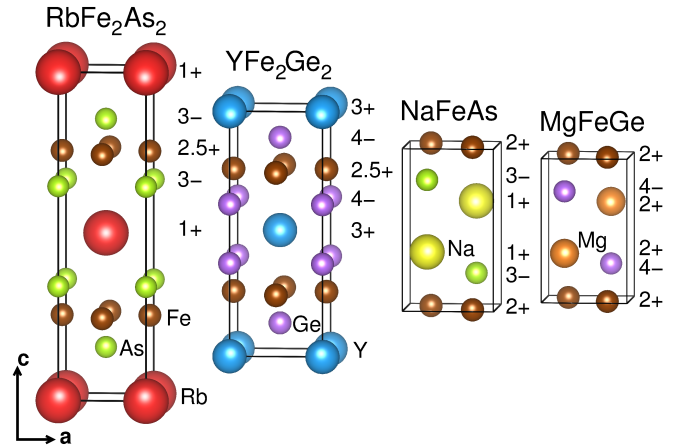


FIG. 1. (Color online) Crystal structures of RbFe<sub>2</sub>As<sub>2</sub>, YFe<sub>2</sub>Ge<sub>2</sub>, NaFeAs and MgFeGe. The unit cells and interatomic distances are true to scale. The numbers next to the unit cells indicate the nominal valence of atoms at the same vertical positions.

but not to the left towards Ge. In agreement with recent NMR measurements [29], our study highlights the role of presence or absence of ferromagnetic fluctuations in determining the value of  $T_c$  in FeBS.

Our analysis shows that conventional low-energy models of FeBS, which only incorporate the Fe  $d$  and  $X$  ( $X=\text{As, Se, Ge, ...}$ )  $p$  states are in some cases not sufficient to explain key features of FeBS. Although these models usually reproduce the Fermi surface very well, they do not reflect the physical instabilities of the actual materials because they neglect the interaction with the spacer between the Fe $X$  layers. Even though bulk FeSe does not contain spacer layers, our arguments may be relevant for intercalates [31–33], alkali-doped thick films [34] and FeSe monolayers on SrTiO<sub>3</sub> [3]

*Materials and Methods.* - We compare isoelectronic iron arsenides and iron germanides from (i) the so-called hole-doped *122-family* where iron is in a nominal oxidation  $\text{Fe}^{2.5+}$  with  $d^{5.5}$  occupation [35–37] and (ii) the so-called *111-family* with  $\text{Fe}^{2+}$  in a  $d^6$  configuration [37–39]. The crystal structures of  $\text{RbFe}_2\text{As}_2$ ,  $\text{YFe}_2\text{Ge}_2$ ,  $\text{NaFeAs}$  and  $\text{MgFeGe}$  are shown in Fig. 1, where we also indicate the nominal valences of the atoms in each compound. Lattice constants and internal positions in this figure were taken from experiment [7, 40–42].

The most obvious structural difference between iron arsenides and iron germanides is shrinking of the  $c$ -axis (Fig. 1). From  $\text{NaFeAs}$  to  $\text{MgFeGe}$  it is not as pronounced as from  $\text{RbFe}_2\text{As}_2$  to  $\text{YFe}_2\text{Ge}_2$ , where Ge  $p_z$ - $p_z$  bonds may form (in  $\text{MgFeGe}$  direct Ge-Ge bonding is not possible). Although these materials are isoelectronic, the germanides have a stronger charge transfer between the Fe $X$  ( $X = \text{As, Ge}$ ) and the spacer layers.

The isoelectronic substitution of As by Ge, Rb by Y, and Na by Mg was simulated within the virtual crystal approximation (VCA). To disentangle effects originating from direct atomic substitution from effects coming from small changes of bond-distances and -angles in real materials, we performed all calculations for the *122-family* with the experimental structural parameters of  $\text{YFe}_2\text{Ge}_2$  [40] and those for the *111-family* with the experimental structural parameters of  $\text{MgFeGe}$  [7]. The technical details of our DFT calculations can be found in Ref. 43.

We also analyze the density of states by using the extended Stoner model [46, 47], which is a simple tool for understanding the origin of itinerant ferromagnetism (see Ref. 43 for details). The paramagnetic state is unstable towards ferromagnetism if the conditions  $1/I = \bar{N}(m)$  and  $0 > d\bar{N}(m)/dm$  are fulfilled at some  $m$ , where  $\bar{N}(m)$  is the paramagnetic density of states averaged over an energy window that contains a sufficient number of states to realize an Fe moment  $m$ , and  $I$  is the Stoner parameter [43].

*Results.* - We first calculated the DFT energies of various spin configurations. By means of the

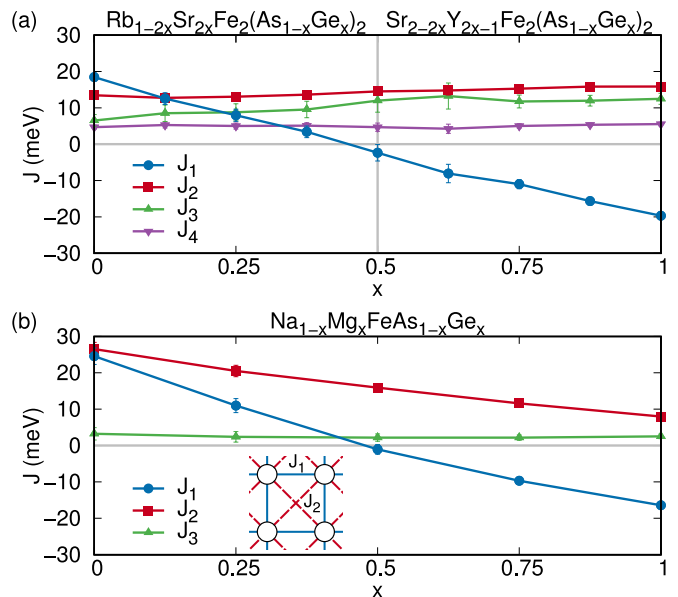


FIG. 2. (Color online) Calculated Heisenberg exchange parameters for (a) the VCA interpolation between  $\text{RbFe}_2\text{As}_2$  and  $\text{YFe}_2\text{Ge}_2$  [via  $\text{SrFe}_2(\text{As}_{0.5}\text{Ge}_{0.5})_2$ ] and (b) the VCA interpolation between  $\text{NaFeAs}$  and  $\text{MgFeGe}$ . Lines are guides to the eye. The error bars represent the statistical errors of the fit. The inset of (b) shows the structure of the two-dimensional Heisenberg model we use to fit the DFT energies.  $J_1$  is the nearest-neighbor coupling in the square lattice of Fe atoms, while  $J_2$  is the next-nearest neighbor coupling.  $J_3$  and  $J_4$  are longer-range exchange couplings. Positive values of  $J$  correspond to antiferromagnetic exchange. Note that all calculations were performed in the crystal structures of  $\text{YFe}_2\text{Ge}_2$  and  $\text{MgFeGe}$  respectively.

VCA we interpolated between  $\text{RbFe}_2\text{As}_2$  and  $\text{YFe}_2\text{Ge}_2$  [via  $\text{SrFe}_2(\text{As}_{0.5}\text{Ge}_{0.5})_2$ ] and between  $\text{NaFeAs}$  and  $\text{MgFeGe}$ . Using a two-dimensional Heisenberg model to parametrize the DFT energies (see Ref. 43 for more details) we observe that the nearest-neighbor exchange coupling  $J_1$  universally changes from antiferromagnetic to ferromagnetic when going continuously from As to Ge without changing the electron count, while all other exchange couplings are almost unaffected (Fig. 2). Only in the *111-family* the next-nearest-neighbor exchange  $J_2$  is also reduced, but it does not change sign. At the germanide end-point the ferromagnetic  $J_1$  becomes the dominant exchange interaction.

Remarkably, we also obtained a large ferromagnetic  $J_1$  for  $\text{NaFeAs}$  after we expanded the structure used for Fig. 2 by 10% along the  $c$ -axis but kept all distances within the FeAs layer unchanged by the expansion. These results indicate that  $\text{NaFeAs}$  can also be turned ferromagnetic by separating the FeAs layers and by shifting Na further away from the layers.

From this analysis we conclude that previous suggestions [15] that iron germanides and iron pnictides show similar magnetic behavior don't hold. While both fam-

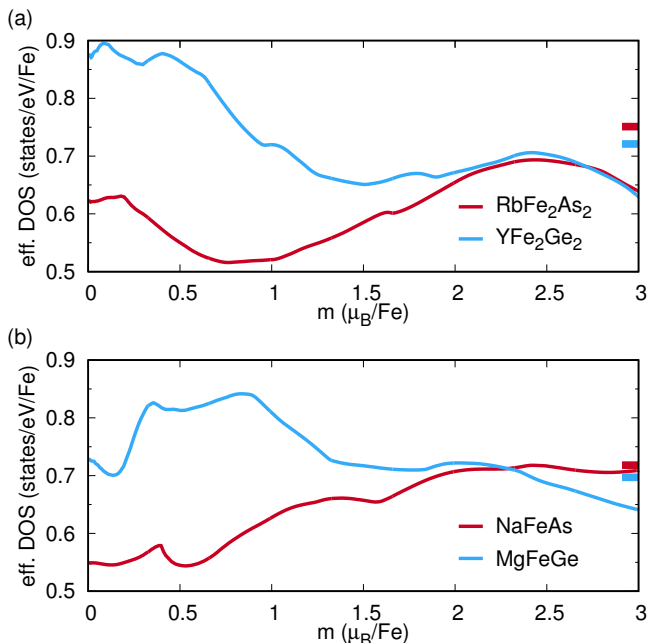


FIG. 3. (Color online) Effective density of states in the extended Stoner model as a function of magnetic moment for (a)  $\text{RbFe}_2\text{As}_2$  and  $\text{YFe}_2\text{Ge}_2$  and (b)  $\text{NaFeAs}$  and  $\text{MgFeGe}$ . The colored bars on the right  $y$ -axis indicate the calculated inverse Stoner parameters  $1/I$  for the respective case. All calculations were performed in the crystal structures of  $\text{YFe}_2\text{Ge}_2$  and  $\text{MgFeGe}$  respectively.

ilies have a stripe antiferromagnetic ground state in the DFT calculations, the nature of excitations is entirely different. This is reflected in the presence of a nearest neighbor ferromagnetic exchange  $J_1$  in iron germanides and antiferromagnetic  $J_1$  in the iron pnictides despite the very similar crystal structure and electronic structure at the Fermi level. In particular, the results on the expanded  $\text{NaFeAs}$  suggest that the origin of this different behavior lies dominantly in the relative separation between the spacer and the  $\text{FeX}$  plane.

A further distinctive feature of the germanides is that the magnetism of Fe in  $\text{YFe}_2\text{Ge}_2$  appears to be rather peculiar. There is a low- and a high-moment solution for Fe, the former more stabilized for shorter Fe-Ge bond length [43] (in pnictides, either a high-spin solution is realized, or magnetism collapses completely).

To understand in a simple framework the origin of the magnetic behavior presented above we investigate the effective density of states  $\bar{N}$  as a function of the magnetic moment  $m$  within the extended Stoner model (see Fig. 3). We observe that (i) iron germanides have in general a higher DOS at the Fermi level and (ii) a significant number of states is shifted from higher energies towards the Fermi level, as compared to pnictides. This is signalled by the strong increase of the effective DOS at low moments (see Fig. 3 where results for  $\text{YFe}_2\text{Ge}_2$  versus  $\text{RbFe}_2\text{As}_2$

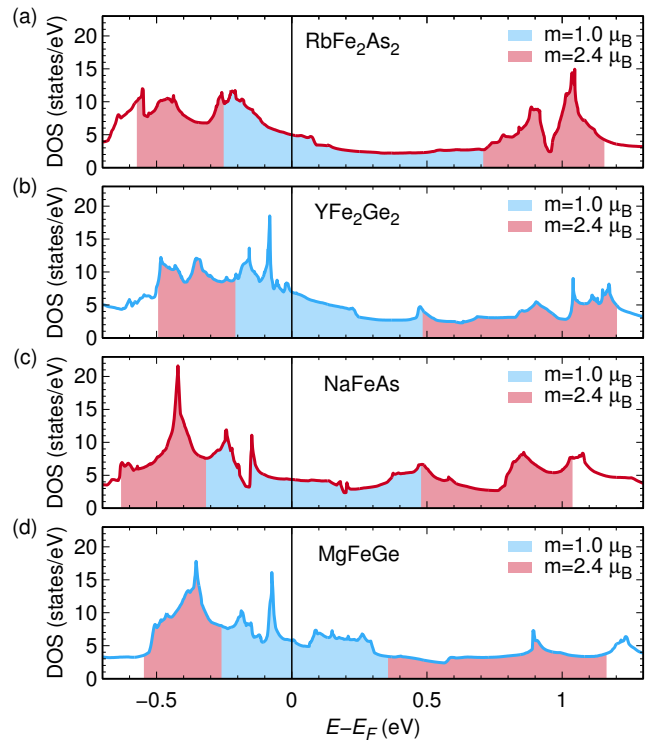


FIG. 4. (Color online) Total density of states calculated from DFT for (a)  $\text{RbFe}_2\text{As}_2$ , (b)  $\text{YFe}_2\text{Ge}_2$ , (c)  $\text{NaFeAs}$  and (d)  $\text{MgFeGe}$ . The shaded areas below the curves correspond to the energy range needed to realize a moment of  $1.0 \mu_B$  or  $2.4 \mu_B$  per iron respectively within the extended Stoner model. All calculations were performed in the crystal structures of  $\text{YFe}_2\text{Ge}_2$  and  $\text{MgFeGe}$  respectively.

and  $\text{MgFeGe}$  versus  $\text{NaFeAs}$  are shown). Interestingly, the changes in the high-moment region ( $m \sim 2.4 \mu_B$ ) are marginal, while they are considerable in the low-moment region ( $m < 1.0 \mu_B$ ). Furthermore, we find that the Stoner parameter  $I$  is almost independent of the material and that  $1/I$  lies between  $0.7 \text{ eV}^{-1}$  and  $0.75 \text{ eV}^{-1}$ . Therefore, by looking for crossings of  $\bar{N}(m)$  with  $1/I$  in Fig. 3, we establish that the extended Stoner criterion for ferromagnetism is fulfilled in iron germanides, but not in pnictides. Moreover, the metastability of different magnetic moments in  $\text{YFe}_2\text{Ge}_2$  is also evident from this analysis, as the effective DOS almost fulfills the extended Stoner criterion also for large moments of about  $2.5 \mu_B$ .

Fig. 4 shows the total calculated DOS for  $\text{RbFe}_2\text{As}_2$  vs.  $\text{YFe}_2\text{Ge}_2$ , and  $\text{NaFeAs}$  vs.  $\text{MgFeGe}$ , where we colored the energy regions corresponding to magnetic moments of  $m = 1.0 \mu_B$  (blue) and  $m = 2.4 \mu_B$  (red) in the extended Stoner model. The energy range corresponding to  $m = 1.0 \mu_B$  is compressed when going from arsenides to germanides, while the energy range corresponding to  $m = 2.4 \mu_B$  even increases marginally in germanides. As the density of states in the window shown is dominated by Fe states, this implies that the bandwidth of some of

the Fe states is selectively reduced in iron germanides, while the overall bandwidth is about constant [43].

*Discussion.*- One of the principal questions in the theory of the Fe-based superconductors is what should be the minimal chemical model to explain the essential physics and, above all, superconductivity. It was recognized that the effective Fe-only (“*d*-only”) model does not work in some materials, but it has been believed so far that the electronic properties of iron-based superconductors were exclusively controlled by the FeX layers ( $X=As, Se, Ge, \dots$ ) as described by the so-called “*pd*-model”. Thereby the role of all other constituents was reduced to charge reservoirs.

We have established in this work that iron germanides have a general tendency towards ferromagnetism which proves detrimental for superconductivity even though the Fermi surface is very similar to that of isoelectronic pnictides. Most importantly, this tendency can be traced down to the flattening of some bands near the Fermi level and a modified electronic bandstructure in a wide range of energies at and away from the Fermi level. Neither the collapse of the *c*-axis, nor the hole-doping of the 122 germanides are essential for the emergence of ferromagnetism. However, the character and position of the intercalating species, normally considered irrelevant and not explicitly included in any theory or model, plays a decisive role.

Our findings have important implications for iron-based superconductivity in general: (i) The Fermi surface geometry and topology is an important, but not the only condition for emerging superconductivity. The character of spin fluctuations, even on the level of the simple ferromagnetic-antiferromagnetic dichotomy, may be qualitatively different in seemingly similar materials. (ii) A quantitative theory of  $T_c$  in iron-based superconductors must include the interaction between all constituents of the unit cell, including, in some cases, the interlayer spacers. (iii) While FeGe layers *per se* are not necessarily ferromagnetic, the fact that they have to be spaced with different elements (*e.g.*, Mg vs. Na, or Y vs. Sr) drives them ferromagnetic. (iv) In a more general way, it does matter what we place next to or on top of an Fe-ligand layer. This observation may be directly related to an apparent role that interfacial effects play in high- $T_c$  Fe chalcogenides, such as FeSe monolayers deposited on specially prepared surfaces or  $K_xFe_{2-y}Se_2$  filaments embedded in the magnetic  $K_2Fe_4Se_5$  phase.

*Acknowledgments.*- DG, HOJ and RV thank the German Research Foundation (Deutsche Forschungsgemeinschaft) for financial support through grant SPP 1458. IIM was supported by ONR through the NRL basic research program and by the Alexander von Humboldt foundation. JKG acknowledges the support of the NRC program at NRL. EB acknowledges funding from Ministerio de Economía y Competitividad vía Grant No. FIS2014-53219-P and from Fundación Ramón Areces and

thanks R. Rurali and X. Cartoixa for early calculations. The authors thank S. L. Bud’ko and P. C. Canfield for helpful discussions.

---

\* guterding@itp.uni-frankfurt.de

† Present address: Department of Computational and Data Sciences and Computational Materials Science Center, George Mason University, 4400 University Drive, Fairfax, VA 22030

- [1] Y. Kamihara, T. Watanabe, M. Hirano, and H. Hosono, *Iron-Based Layered Superconductor  $La[O_{1-x}F_x]FeAs$  ( $x = 0.05-0.12$ ) with  $T_c = 26$  K*, J. Am. Chem. Soc. **130**, 3296 (2008).
- [2] H. Hosono and K. Kuroki, *Iron-based superconductors: Current status of materials and pairing mechanism*, Physica C **514**, 399 (2015).
- [3] J.-F. Ge, Z.-L. Liu, C. Liu, C.-L. Gao, D. Qian, Q.-K. Xue, Y. Liu, and J.-F. Jia, *Superconductivity above 100 K in single-layer FeSe films on doped  $SrTiO_3$* , Nat. Mater. **11**, 285 (2015).
- [4] M. A. Avila, S. L. Bud’ko, and P. C. Canfield, *Anisotropic magnetization, specific heat and resistivity of  $RFe_2Ge_2$  single crystals*, J. Magn. Magn. Mater. **270**, 51 (2004).
- [5] S. Ran, S. L. Bud’ko, and P. C. Canfield, *Effects of substitution on low-temperature physical properties of  $LuFe_2Ge_2$* , Philos. Mag. **91**, 4388 (2011).
- [6] H. Kim, S. Ran, E. D. Mun, H. Hodovanets, M. A. Tanatar, R. Prozorov, S. L. Bud’ko, and P. C. Canfield, *Crystal growth and annealing study of fragile, non-bulk superconductivity in  $YFe_2Ge_2$* , Philos. Mag. **95**, 804 (2015).
- [7] Y. Liu, S. Matsuishi, S. Fujitsu, and H. Hosono, *MgFeGe is an isoelectronic and isostructural analog of the superconductor  $LiFeAs$* , Phys. Rev. B **85**, 104403 (2012).
- [8] Y. Zou, Z. Feng, P. W. Logg, J. Chen, G. Lampronti, and F. M. Grosche, *Fermi liquid breakdown and evidence for superconductivity in  $YFe_2Ge_2$* , Phys. Status Solidi RRL **8**, 928 (2014).
- [9] J. Chen, K. Semeniuk, Z. Feng, P. Reiss, P. Brown, Y. Zou, P. W. Logg, G. I. Lampronti, and F. M. Grosche, *Unconventional Superconductivity in the Layered Iron Germanide  $YFe_2Ge_2$* , Phys. Rev. Lett. **116**, 127001 (2016).
- [10] A. Subedi, *Unconventional sign-changing superconductivity near quantum criticality in  $YFe_2Ge_2$* , Phys. Rev. B **89**, 024504 (2014).
- [11] D. J. Singh, *Superconductivity and magnetism in  $YFe_2Ge_2$* , Phys. Rev. B **89**, 024505 (2014).
- [12] J.-J. Ying, L.-Y. Tang, V. V. Struzhkin, H.-K. Mao, A. G. Gavriliuk, A.-F. Wang, X.-H. Chen, and X.-J. Chen, *Tripling the critical temperature of  $KFe_2As_2$  by carrier switch*, arXiv:1501.00330 (unpublished).
- [13] Y. Nakajima, R. Wang, T. Metz, X. Wang, L. Wang, H. Cynn, S. T. Weir, J. R. Jeffries, and J. Paglione, *High-temperature superconductivity stabilized by electron-hole interband coupling in collapsed tetragonal phase of  $KFe_2As_2$  under high pressure*, Phys. Rev. B **91**, 060508(R) (2015).
- [14] D. Guterding, S. Backes, H. O. Jeschke, and R. Valentí, *Origin of the superconducting state in the col-*

- lapsed tetragonal phase of  $KFe_2As_2$* , Phys. Rev. B **91**, 140503(R) (2015).
- [15] G. Wang and X. Shi, *Electronic structures and magnetism of  $YM_2Ge_2$  ( $M = Mn-Cu$ ): Ge-height dependent magnetic ordering in  $YFe_2Ge_2$* , Comput. Mater. Sci. **121**, 48 (2016).
- [16] N. Sirica, F. Bondino, S. Nappini, I. Piš, L. Poudel, A. D. Christianson, D. Mandrus, D. J. Singh, and N. Mannella, *Spectroscopic evidence for strong quantum spin fluctuations with itinerant character in  $YFe_2Ge_2$* , Phys. Rev. B **91**, 121102(R) (2015).
- [17] D. F. Xu, D. W. Shen, D. Zhu, J. Jiang, B. P. Xie, Q. S. Wang, B. Y. Pan, P. Dudin, T. K. Kim, M. Hoesch, J. Zhao, X. G. Wan, and D. L. Feng, *Electronic structure of  $YFe_2Ge_2$  studied by angle-resolved photoemission spectroscopy*, Phys. Rev. B **93**, 024506 (2016).
- [18] P. J. Hirschfeld, M. M. Korshunov, and I. I. Mazin, *Gap symmetry and structure of Fe-based superconductors*, Rep. Prog. Phys. **74**, 124508 (2011).
- [19] A. Chubukov, *Pairing Mechanism in Fe-Based Superconductors*, Annu. Rev. Condens. Matter Phys. **3**, 57 (2012).
- [20] J. C. S. Davis and D.-H. Lee, *Concepts relating magnetic interactions, intertwined electronic orders, and strongly correlated superconductivity*, Proc. Natl. Acad. Sci. USA **110**, 17623 (2013).
- [21] J. K. Glasbrenner, I. I. Mazin, H. O. Jeschke, P. J. Hirschfeld, R. M. Fernandes, and R. Valentí, *Effect of magnetic frustration on nematicity and superconductivity in Fe chalcogenides*, Nat. Phys. **11**, 953 (2015).
- [22] Q. Si, R. Yu, and E. Abrahams, *High-temperature superconductivity in iron pnictides and chalcogenides*, Nature Reviews Materials **1**, 16017 (2016).
- [23] J. Hu, *Identifying the genes of unconventional high temperature superconductors*, Sci. Bull. **61**, 561 (2016).
- [24] D. Guterding, S. Backes, M. Tomić, H. O. Jeschke, and R. Valentí, *Ab-initio perspective on structural and electronic properties of iron-based superconductors*, Phys. Status Solidi B (in press), arXiv:1606.04411.
- [25] E. Bascones, B. Valenzuela, and M. J. Calderón, *Comptes Rendus Physique* **17**, 36 (2016).
- [26] H. O. Jeschke, I. I. Mazin, and R. Valentí, *Why  $MgFeGe$  is not a superconductor*, Phys. Rev. B **87**, 241105(R) (2013).
- [27] Z. P. Yin, K. Haule, and G. Kotliar, *Spin dynamics and orbital-antiphase pairing symmetry in iron-based superconductors*, Nat. Phys. **10**, 845 (2014).
- [28] M.-C. Ding and Y.-Z. Zhang, *Possible way to turn  $MgFeGe$  into an iron-based superconductor*, Phys. Rev. B **89**, 085120 (2014).
- [29] P. Wiecki, B. Roy, D. C. Johnston, S. L. Bud'ko, P. C. Canfield, and Y. Furukawa, *Competing Magnetic Fluctuations in Iron Pnictide Superconductors: Role of Ferromagnetic Spin Correlations Revealed by NMR*, Phys. Rev. Lett. **115**, 137001 (2015).
- [30] W. Li, H. Ding, Z. Li, P. Deng, K. Chang, K. He *et al.*,  *$KFe_2Se_2$  is the Parent Compound of K-Doped Iron Selenide Superconductors*, Phys. Rev. Lett. **109**, 057003 (2012).
- [31] M. Burrard-Lucas, D. G. Free, S. J. Sedlmaier, J. D. Wright, S. J. Cassidy, Y. Hara, A. J. Corkett, T. Lancaster, P. J. Baker, S. J. Blundell, and S. J. Clarke, *Enhancement of the superconducting transition temperature of  $FeSe$  by intercalation of a molecular spacer layer*, Nat. Mater. **12**, 15 (2013).
- [32] D. Guterding, H. O. Jeschke, P. J. Hirschfeld, and R. Valentí, *Unified picture of the doping dependence of superconducting transition temperatures in alkali metal/ammonia intercalated  $FeSe$* , Phys. Rev. B **91**, 041112(R) (2015).
- [33] H. Sun, D. N. Woodruff, S. J. Cassidy, G. M. Allcroft, S. J. Sedlmaier, A. L. Thompson, P. A. Bingham, S. D. Forder, S. Cartenet, N. Mary, S. Ramos, F. R. Foronda, B. J. Williams, X. Li, S. J. Blundell, and S. J. Clarke, *Soft Chemical Control of Superconductivity in Lithium Iron Selenide Hydroxides  $Li_{1-x}Fe_x(OH)Fe_{1-y}Se$* , Inorg. Chem. **54**, 1958 (2015).
- [34] C. H. P. Wen, H. C. Xu, C. Chen, Z. C. Huang, X. Lou, Y. K. Pu *et al.*, *Anomalous correlation effects and unique phase diagram of electron-doped  $FeSe$  revealed by photoemission spectroscopy*, Nat. Commun. **7**, 10840 (2016).
- [35] S. Backes, D. Guterding, H. O. Jeschke, and R. Valentí, *Electronic structure and de Haas-van Alphen frequencies in  $KFe_2As_2$  within LDA+DMFT*, New J. Phys. **16**, 085025 (2014).
- [36] S. Backes, H. O. Jeschke, and R. Valentí, *Microscopic nature of correlations in multi-orbital  $AFe_2As_2$  ( $A = K, Rb, Cs$ ): Hund's coupling versus Coulomb repulsion*, Phys. Rev. B **92**, 195128 (2015).
- [37] Z. P. Yin, K. Haule, and G. Kotliar, *Kinetic frustration and the nature of the magnetic and paramagnetic states in iron pnictides and iron chalcogenides*, Nat. Mater. **10**, 932 (2011).
- [38] J. Ferber, K. Foyevtsova, R. Valentí, and H. O. Jeschke, *LDA+DMFT study of the effects of correlation in  $LiFeAs$* , Phys. Rev. B **85**, 094505 (2012).
- [39] G. Lee, H. S. Ji, Y. Kim, C. Kim, K. Haule, G. Kotliar, B. Lee, S. Khim, K. H. Kim, K. S. Kim, K.-S. Kim, and J. H. Shim, *Orbital Selective Fermi Surface Shifts and Mechanism of High  $T_c$  Superconductivity in Correlated  $AFeAs$  ( $A=Li, Na$ )*, Phys. Rev. Lett. **109**, 177001 (2012).
- [40] G. Venturini and B. Malaman, *X-ray single crystal refinements on some  $RT_2Ge_2$  compounds ( $R = Ca, Y, La, Nd, U$ ;  $T = Mn-Cu, Ru-Pd$ ): evolution of the chemical bonds*, J. Alloys Compd. **235**, 201 (1996).
- [41] D. R. Parker, M. J. Pitcher, P. J. Baker, I. Franke, T. Lancaster, S. J. Blundell, and S. J. Clarke, *Structure, antiferromagnetism and superconductivity of the layered iron arsenide  $NaFeAs$* , Chem. Commun. **16**, 2189 (2009).
- [42] F. Eilers, K. Grube, D. A. Zocco, T. Wolf, M. Merz, P. Schweiss, R. Heid, R. Eder, R. Yu, J.-X. Zhu, Q. Si, T. Shibauchi, and H. v. Löhneysen, *Strain-Driven Approach to Quantum Criticality in  $AFe_2As_2$  with  $A = K, Rb$ , and  $Cs$* , Phys. Rev. Lett. **116**, 237003 (2016).
- [43] See Supplemental Material at [URL inserted by publisher], which provides additional information on the metastability of magnetic moments, details of the extended Stoner analysis and electronic bandstructures with orbital weights for the VCA calculation. The supplement includes Ref. [44] and [45].
- [44] K. Koepf and H. Eschrig, *Full-potential nonorthogonal local-orbital minimum-basis band-structure scheme*, Phys. Rev. B **59**, 1743 (1999); <http://www.FPLO.de>
- [45] J. P. Perdew, K. Burke, and M. Ernzerhof, *Generalized Gradient Approximation Made Simple*, Phys. Rev. Lett. **77**, 3865 (1996).
- [46] O. K. Andersen, J. Madsen, U. K. Poulsen, O. Jepsen, and J. Kollár, *Magnetic ground state properties of transition metals*, Physica B+C **86-88**, 249 (1977).

- [47] I. I. Mazin and D. J. Singh, *Electronic structure and magnetism in Ru-based perovskites*, Phys. Rev. B **56**, 2556 (1997).

# Supplemental Information: Non-trivial role of interlayer cation states in iron-based superconductors

Daniel Guterding,<sup>1,\*</sup> Harald O. Jeschke,<sup>1</sup> I. I. Mazin,<sup>2</sup> J. K. Glasbrenner,<sup>3,†</sup> E. Bascones,<sup>4</sup> and Roser Valentí<sup>1</sup>

<sup>1</sup>*Institut für Theoretische Physik, Goethe-Universität Frankfurt,  
Max-von-Laue-Straße 1, 60438 Frankfurt am Main, Germany*

<sup>2</sup>*Code 6393, Naval Research Laboratory, Washington, DC 20375, USA*

<sup>3</sup>*National Research Council/Code 6393, Naval Research Laboratory, Washington, DC 20375, USA*

<sup>4</sup>*Instituto de Ciencia de Materiales de Madrid, ICMM-CSIC, Cantoblanco, 28049 Madrid, Spain*

## I. METASTABILITY OF MAGNETIC STATES WITH DIFFERENT ORDERED MOMENTS IN $\text{YFe}_2\text{Ge}_2$

We analyzed the energies of different magnetic configurations in  $\text{YFe}_2\text{Ge}_2$  using the FPLO density functional theory code<sup>1</sup> with a GGA exchange-correlation functional<sup>2</sup>, following Refs. 3–5. We investigate the GGA+U ordered moment of  $\text{YFe}_2\text{Ge}_2$  as a function of the Fe-Ge bond length, starting with  $U = 0$ . For the magnetic order we choose ferromagnetic arrangement within the iron plane and antiferromagnetic stacking along the  $c$ -axis. We find that  $\text{YFe}_2\text{Ge}_2$  shows a peculiar metastability of ordered magnetic states with ordered moments of  $m \sim 1\mu_B$  (low moment) and  $m \sim 2\mu_B$  (high moment). The ground state for small Fe-Ge bond lengths has an ordered moment of about  $m \sim 1\mu_B$ , while the  $m \sim 2\mu_B$  state can be stabilized for larger Fe-Ge bond lengths. The results are summarized in Fig. 1. Note that some of the solutions initialized as high moment actually converged to a low moment solution.

Furthermore, we investigated the influence of Coulomb repulsion on the Fe  $3d$  orbitals. We find that even a tiny Coulomb repulsion  $U = 0.25$  eV is sufficient to make the high moment compete for the global energy minimum. The

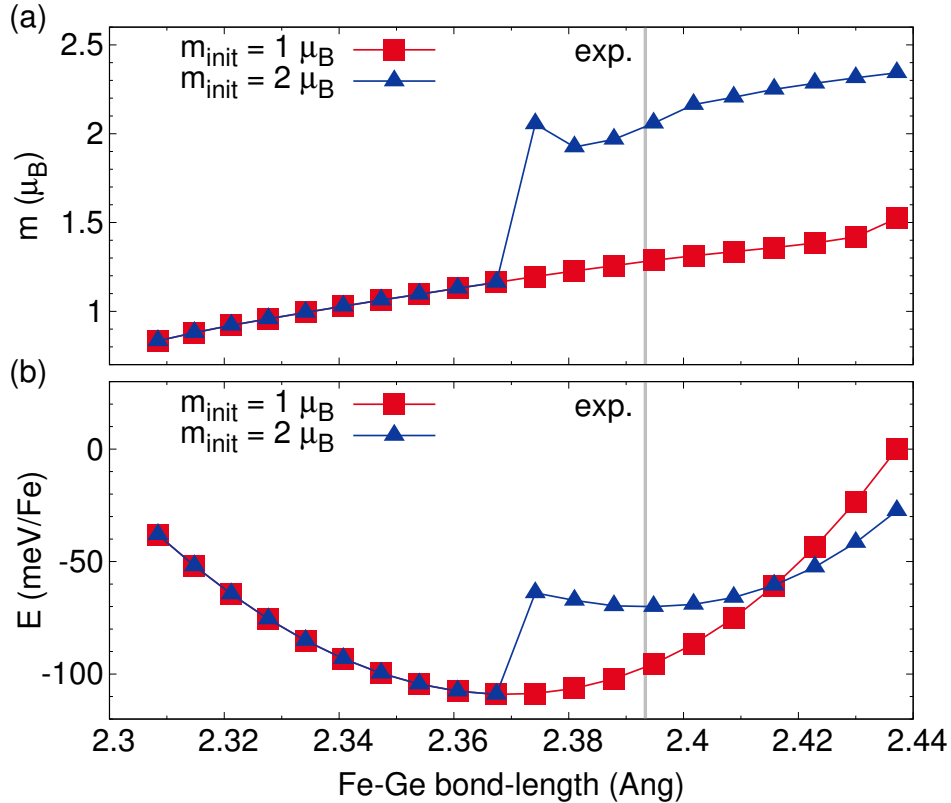


FIG. 1. (a) Magnetic moment versus Fe-Ge bond length and (b) total energy versus Fe-Ge bond length for  $\text{YFe}_2\text{Ge}_2$ . All calculations were performed with GGA xc-functional. The red curve was generated from ferromagnetic initial configurations within the Fe plane with a moment of  $1\mu_B$  per Fe. The ferromagnetic planes were stacked antiferromagnetically in the  $c$ -direction. Calculations with an initial magnetic moment of  $2\mu_B$  per Fe result in the blue curve. The vertical grey line marks the experimental Fe-Ge bond-length.

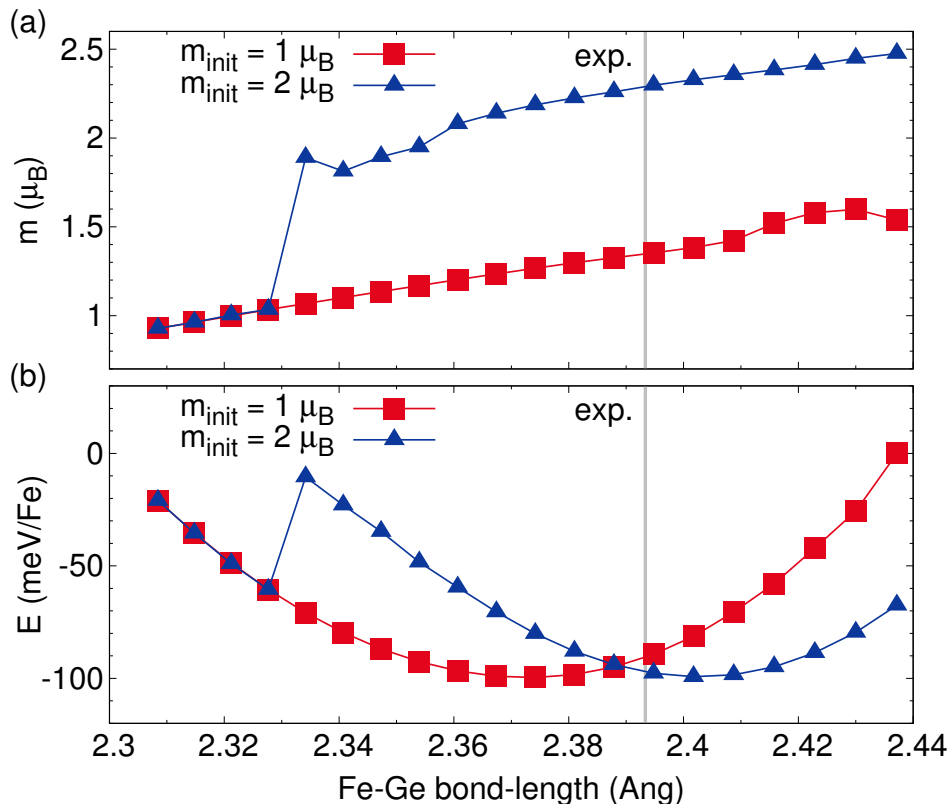


FIG. 2. (a) Magnetic moment versus Fe-Ge bond length and (b) total energy versus Fe-Ge bond length for  $\text{YFe}_2\text{Ge}_2$ . All calculations were performed with GGA+U xc-functional using  $U = 0.25$  eV. The red curve was generated from ferromagnetic initial configurations within the Fe plane with a moment of  $1\mu_B$  per Fe. The ferromagnetic planes were stacked antiferromagnetically in the  $c$ -direction. Calculations with an initial magnetic moment of  $2\mu_B$  per Fe result in the blue curve. The vertical grey line marks the experimental Fe-Ge bond-length.

results for this calculation are summarized in Fig. 2. Note that a larger Coulomb repulsion also shifts the minimum in the energy for the high-moment solutions to larger Fe-Ge bond lengths.

The metastability of low- and high-moment solutions lead us to the investigation of the germanide compounds within the extended Stoner formalism.

## II. METASTABILITY OF MAGNETIC STATES WITH DIFFERENT ORDERED MOMENTS IN $\text{MgFeGe}$

Using the Wien2k code and otherwise comparable calculation setup we also investigated the energy of the low- and high-moment solution in  $\text{MgFeGe}$  as a function of the Ge height. Depending on the Ge height, either the low- or the high-spin solution is stable, and the other solution manifests itself as a shoulder (inflection point) in the  $E(M)$  curve. This behavior is shown in Fig. 3, which shows the values of the magnetic moment  $M$  at the energy minimum and the inflection point as a function of the Ge  $z$ -position.

## III. EXTENDED STONER MODEL

In the extended Stoner calculation we follow Ref. 6. The extended Stoner theory determines whether the paramagnetic state of a material is stable against ferromagnetism.

Within the extended Stoner theory the total magnetization energy can be written as Eq. 1, where  $m$  is the magnetization and  $\bar{N}(m)$  is the density of states averaged between the Fermi levels of the spin-up and the spin-down channels. In the limit of  $m \rightarrow 0$  the effective Stoner DOS is simply the total DOS at the Fermi level. For all other moments  $m$  the effective Stoner DOS is the average total DOS within an increasingly large energy window around the Fermi



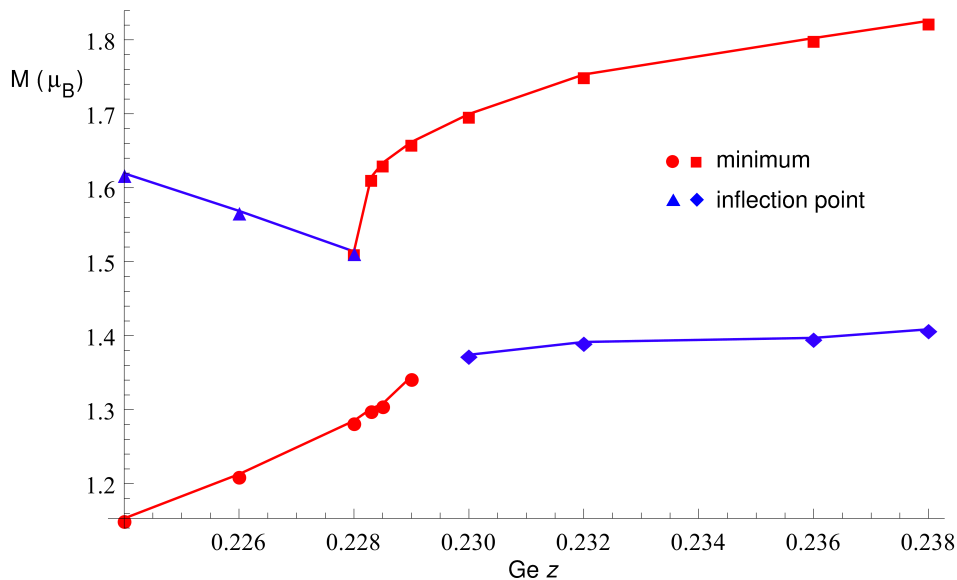


FIG. 3. Magnetic moment  $M$  at the minimum and the inflection point of the  $E(M)$  curve from fixed-moment calculations in MgFeGe as a function of the Ge  $z$ -position (Ge height). The energy minimum changes from the low-spin to the high-spin solution when Ge height is increased beyond a certain value. Lines are guides to the eye.

energy. The density of states is evaluated within the rigid-band approximation starting from the paramagnetic state.

$$E(m) = \frac{1}{2} \int_0^m \frac{m' dm'}{\bar{N}(m')} - \frac{Im^2}{4} \quad (1)$$

The first term is the one-electron energy, because the change in energy for a single electron upon generating a moment  $m$  is half the energy difference  $\Delta(m)$  between the Fermi levels of the spin-up and spin-down channels. Using  $\Delta(m)\bar{N}(m) = m$  one obtains Eq. 2. Integrating this expression one obtains the first term in Eq. 1.

$$\frac{dE}{dm} = \frac{\Delta(m)}{2} = \frac{m}{2\bar{N}(m)} \quad (2)$$

The second term is the so-called Stoner parameter, which parametrizes the ferromagnetic exchange-interactions between electrons in an averaged form.

Now we derive the conditions under which the paramagnetic state is unstable towards ferromagnetism. We start by finding the extrema in the energy for Eq. 1. These are given by Eq. 3.

$$0 \stackrel{!}{=} \frac{dE}{dm} = \bar{N}(m)^{-1} - I \quad (3)$$

Next we find the condition under which this extremum is a minimum in the magnetization energy. It is given by Eq. 4, where we used  $I = \bar{N}(m)^{-1}$ .

$$0 < \stackrel{!}{=} \frac{d^2E}{dm^2} = \frac{1}{2\bar{N}(m)} - m \frac{d\bar{N}(m)/dm}{2\bar{N}(m)^2} - \frac{I}{2} = -m \frac{d\bar{N}(m)/dm}{2\bar{N}(m)^2} \quad (4)$$

As all moments  $m$  and effective densities of states are positive, the resulting condition is  $0 > d\bar{N}(m)/dm$ .

Combining Eqs. 3 and 4 we find that the paramagnetic state is unstable towards ferromagnetism if the conditions  $1 = \bar{N}(m)I$  and  $0 > d\bar{N}(m)/dm$  are fulfilled for the same value of  $m$ .

The Stoner parameter  $I$  can be obtained from fixed-moment DFT calculations by inserting the DFT energies for  $E(m)$  into Eq. 1, using the paramagnetic DFT density of states to calculate  $\bar{N}(m)$  and performing a numerical optimization to obtain the value of  $I$  on the parabolic term in Eq. 1. The effective Stoner parameter  $I$  was calculated from a fit to DFT total energies of ferromagnetic configurations with a moment of up to  $3 \mu_B$  per iron site. All calculations for the Stoner analysis were converged using  $20^3$   $k$ -point grids.

The results are shown in Fig. 4. The values for the Stoner parameters are 1.331 eV (RbFe<sub>2</sub>As<sub>2</sub> in YFe<sub>2</sub>Ge<sub>2</sub> structure), 1.388 eV (YFe<sub>2</sub>Ge<sub>2</sub>), 1.392 eV (NaFeAs in MgFeGe structure) and 1.435 (MgFeGe). Note that the fit is good in the high moment region. The deviation for low moments probably originates from an admixture of non-Fe states, which increases the effective Stoner parameter. This would also explain why the fit is generally worse for germanide compounds, where also a significant amount of interlayer cation states is at the Fermi level. As we use extended Stoner theory only as a qualitative tool, these discrepancies are of minor importance.

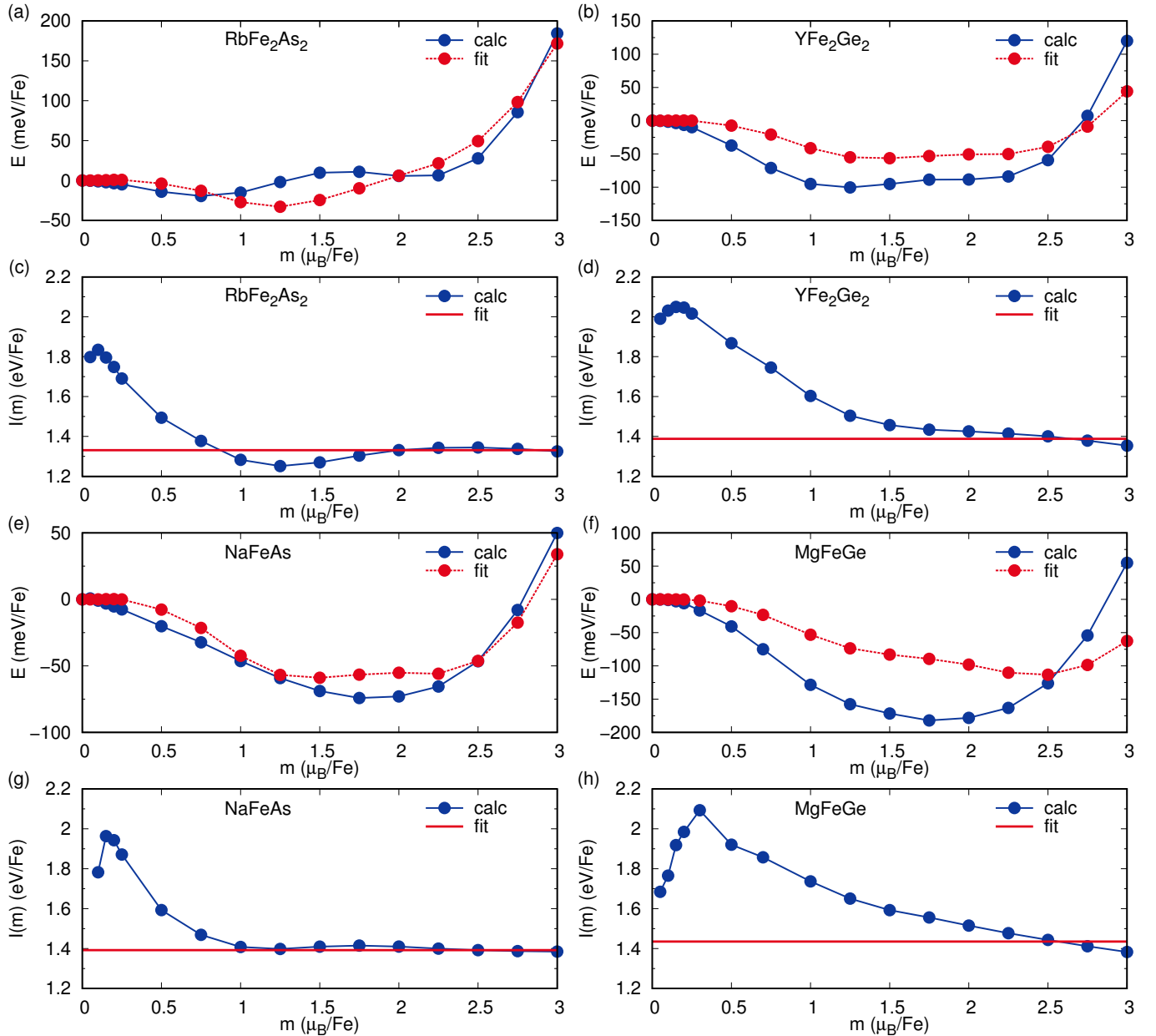


FIG. 4. (a),(b),(e),(f) Fit of Eq. 1 to the fixed-moment energies calculated from DFT. (c),(d),(g),(h) Same data as in (a),(b),(e),(f) after subtracting the one-electron energies (first term in Eq. 1) and dividing by  $-m^2/4$ .

#### IV. DETAILS ON CALCULATION OF HEISENBERG EXCHANGE PARAMETERS

We calculate the magnetic exchange interactions based on a  $2 \times 2 \times 1$  supercell containing eight Fe atoms. This leads to 17 inequivalent magnetic configurations for the *122-compounds* and 13 inequivalent configurations for the *111-compounds*. We used  $8^3$   $k$ -point grids for converging these magnetic calculations. The Heisenberg exchange couplings were extracted by mapping DFT total energies of all inequivalent magnetic configurations to a classical Heisenberg model for each composition.

#### V. ELECTRONIC STRUCTURE FOR VCA INTERPOLATION BETWEEN NaFeAs AND MgFeGe

We investigate the changes in electronic structure when continuously turning MgFeGe into NaFeAs using the virtual crystal approximation, while keeping all structural parameters constant. The electronic bandstructures with orbital weights are shown in Figs. 5, 6 and 7.

The flattening of bands described in the main text can be seen in Fig. 5, where the Fe  $d_{xz}$  states at the  $X$ -point are lowered almost to the Fermi level in MgFeGe and the corresponding band becomes very flat. In the same figure one can see that the Fe  $d_{xy}$  states in turn increase their bandwidth when going from NaFeAs to MgFeGe, for example by comparing the path segment  $M$ - $\Gamma$ . Fig. 7 shows that the cation states are lowered very much in energy, for example at the  $M$ -point. Furthermore, their weight at the lower end of the energy range shown increases when going from NaFeAs to MgFeGe.

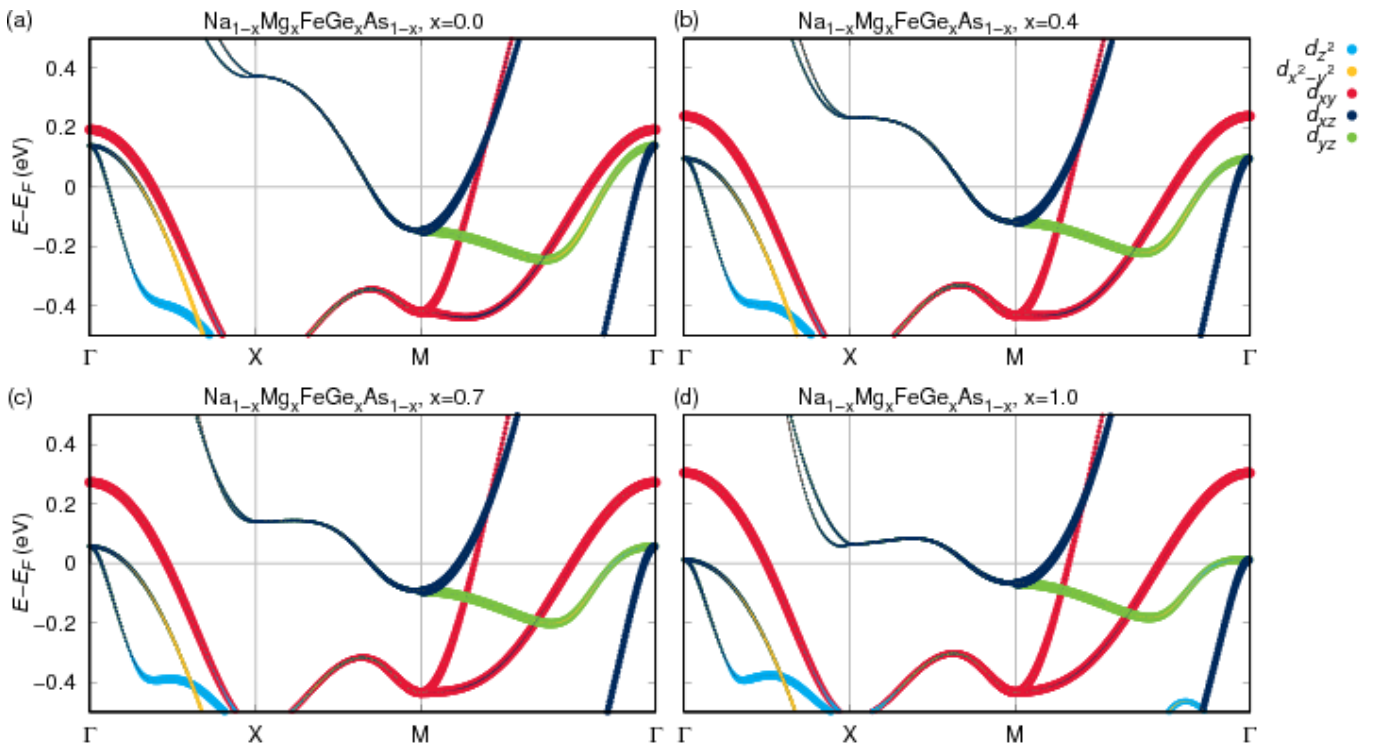


FIG. 5. Electronic bandstructure for the VCA interpolation between NaFeAs and MgFeGe. Colors indicate the weights of Fe  $3d$  orbitals.

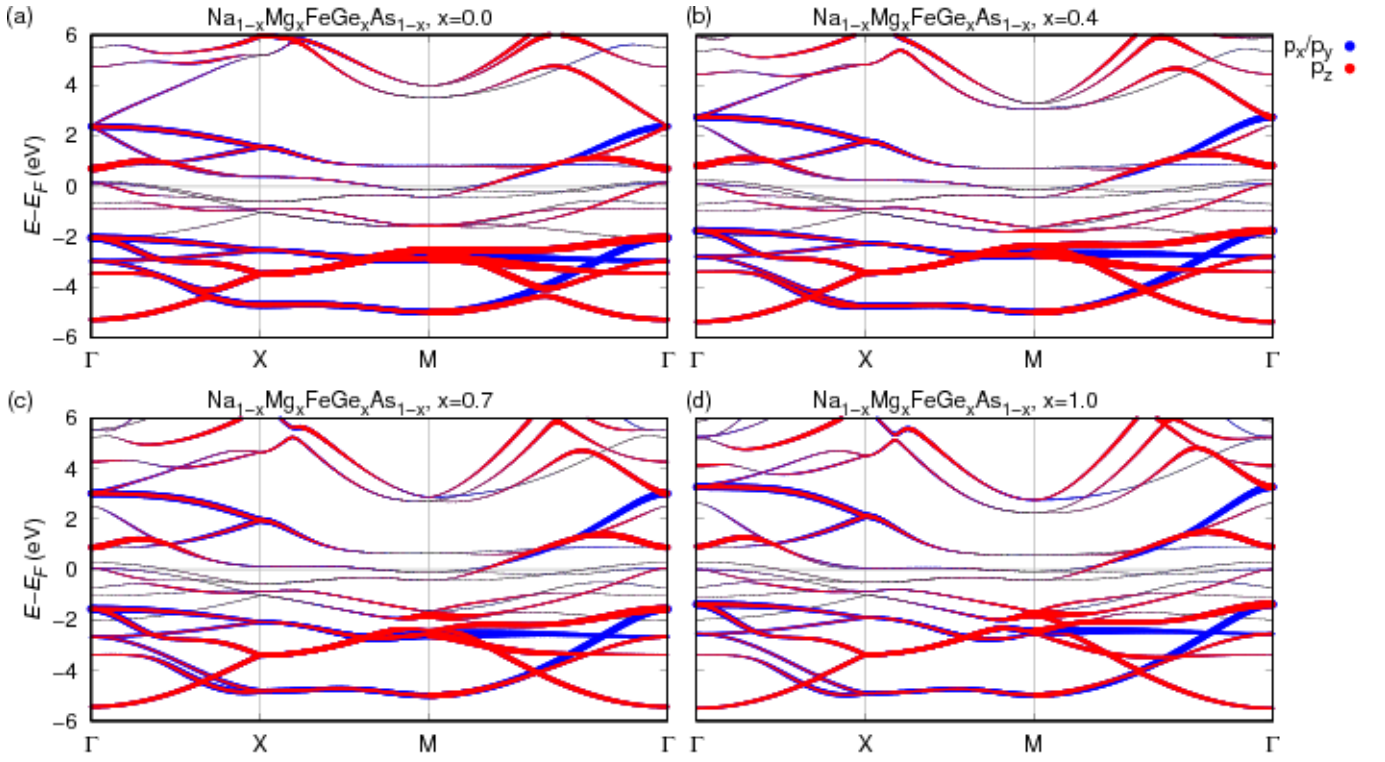


FIG. 6. Electronic bandstructure for the VCA interpolation between NaFeAs and MgFeGe. Colors indicate the weights of As/Ge 4p orbitals.

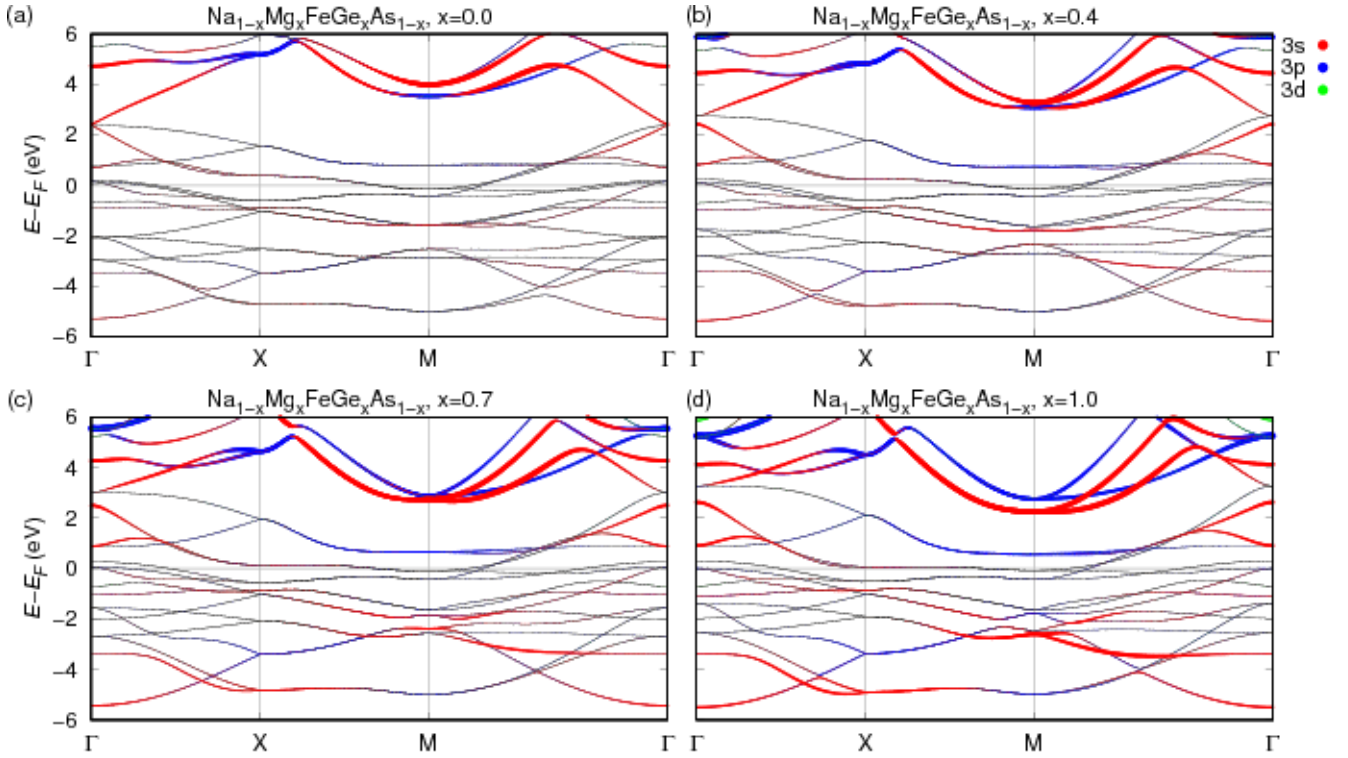


FIG. 7. Electronic bandstructure for the VCA interpolation between NaFeAs and MgFeGe. Colors indicate the weights of Na/Mg 3s, 3p and 3d orbitals.

## VI. ELECTRONIC STRUCTURE FOR VCA INTERPOLATION BETWEEN $\text{RbFe}_2\text{As}_2$ AND $\text{YFe}_2\text{Ge}_2$

We investigate the changes in electronic structure when continuously turning  $\text{YFe}_2\text{Ge}_2$  into  $\text{RbFe}_2\text{As}_2$  using the virtual crystal approximation, while keeping all structural parameters constant. The VCA calculation is carried out starting from strontium on the yttrium/rubidium site. The electronic bandstructures with orbital weights are shown in Figs. 8, 9 and 10.

The flattening of bands described in the main text can be seen in Fig. 8. Here it is most pronounced as a flattening of Fe  $3d_{xz/yz}$  states on the  $M$ - $\Gamma$  path segment. The effect of cation substitution on the position of the As/Ge  $4p_z$  at the  $\Gamma$ -point is very strong here, as can be seen in Fig. 9 at the lower end of the energy window. Fig. 10 shows that the cation states are lowered very much in energy, for example at the  $\Gamma$ -point. Furthermore, their weight at the Fermi level strongly increases when going from  $\text{RbFe}_2\text{As}_2$  to  $\text{YFe}_2\text{Ge}_2$ .

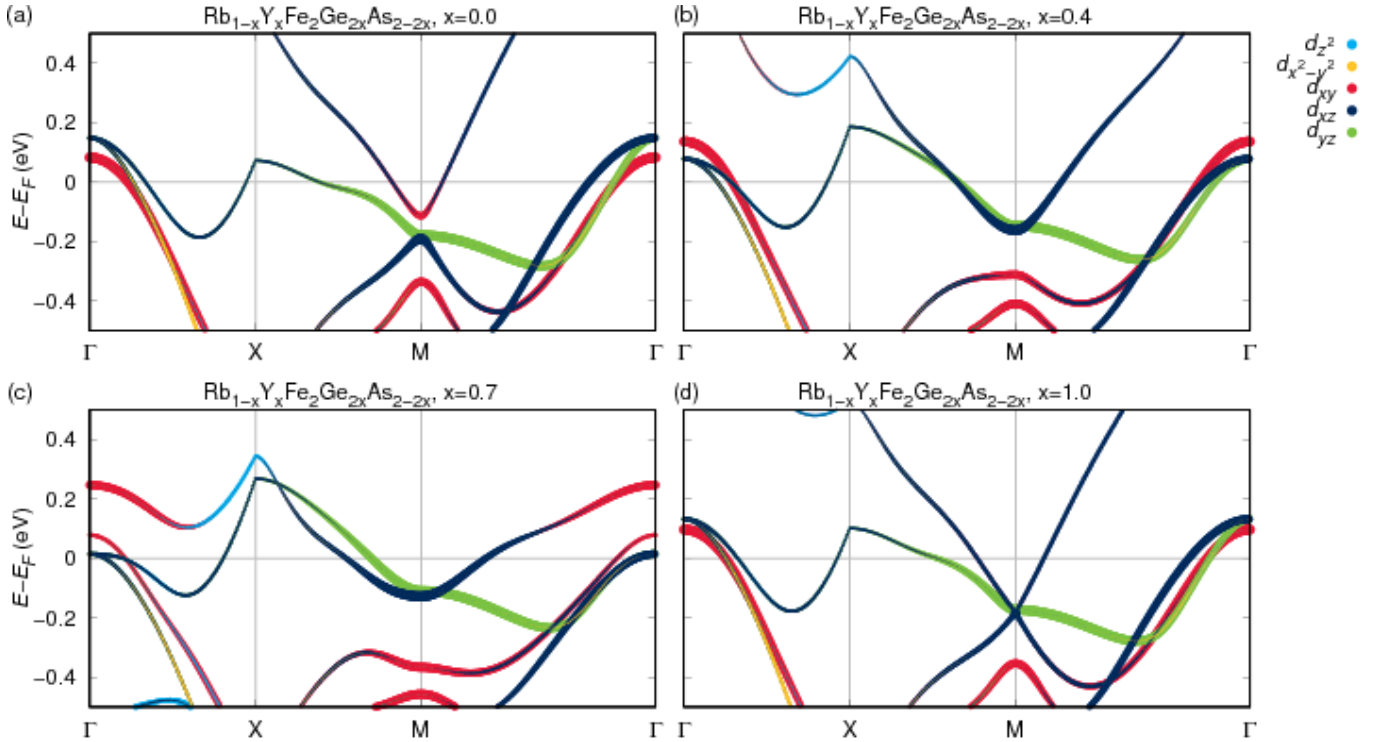


FIG. 8. Electronic bandstructure for the VCA interpolation between  $\text{RbFe}_2\text{As}_2$  and  $\text{YFe}_2\text{Ge}_2$ . Colors indicate the weights of Fe  $3d$  orbitals.

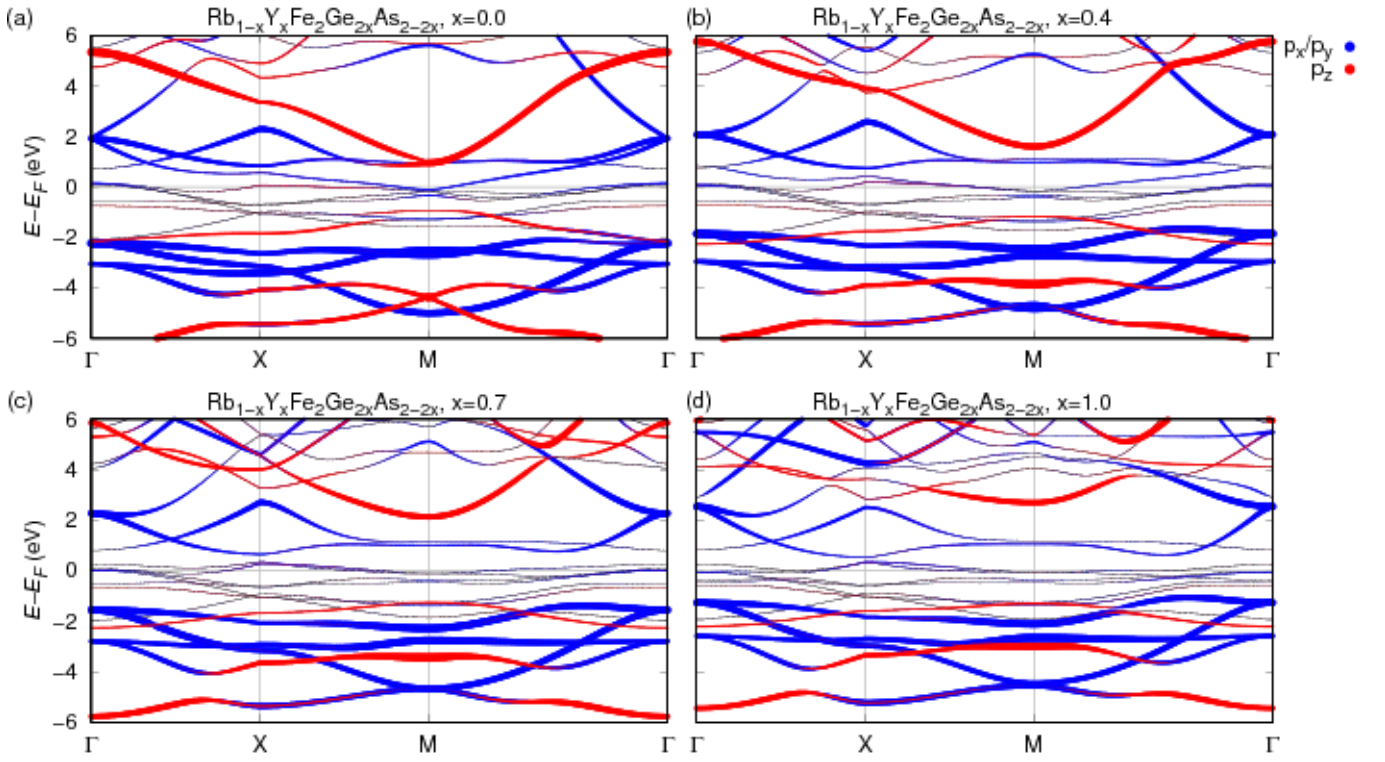


FIG. 9. Electronic bandstructure for the VCA interpolation between  $\text{RbFe}_2\text{As}_2$  and  $\text{YFe}_2\text{Ge}_2$ . Colors indicate the weights of As/Ge  $4p$  orbitals.

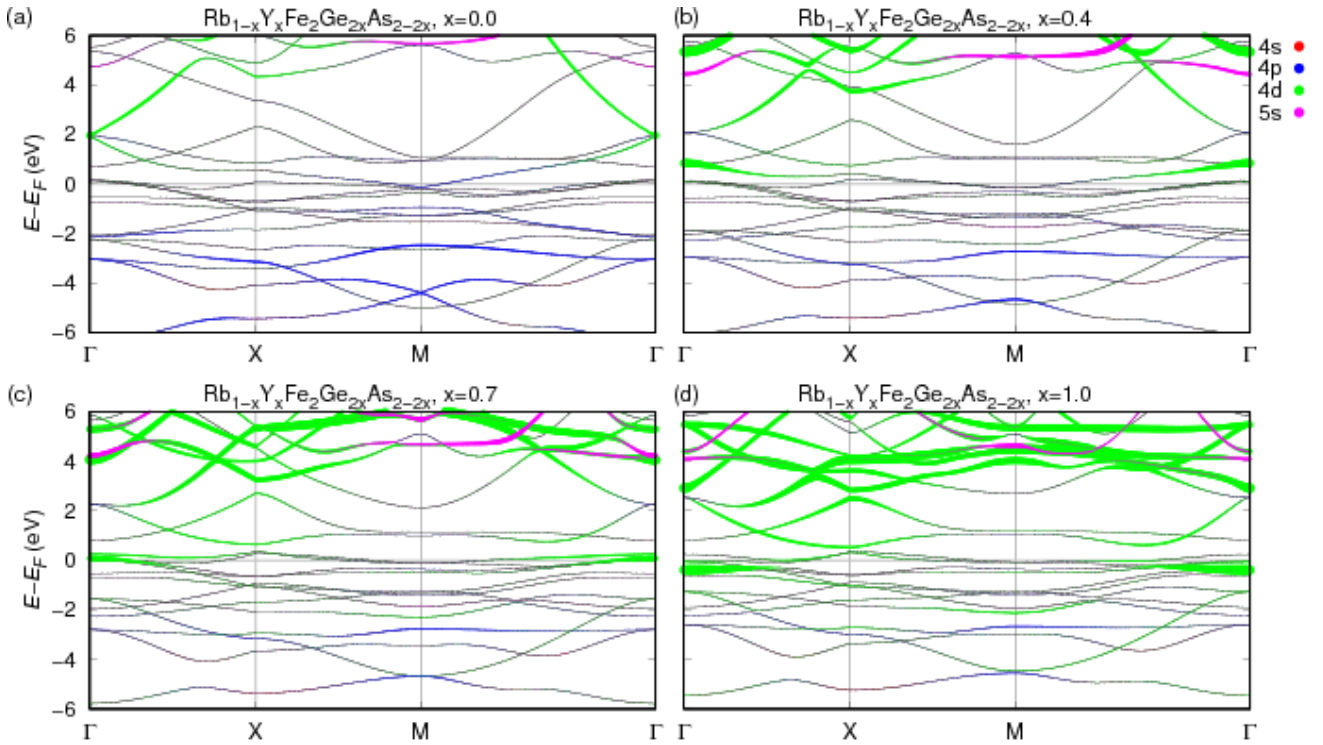


FIG. 10. Electronic bandstructure for the VCA interpolation between  $\text{RbFe}_2\text{As}_2$  and  $\text{YFe}_2\text{Ge}_2$ . Colors indicate the weights of Rb/Y  $4s$  and  $4d$  orbitals.

---

\* guterding@itp.uni-frankfurt.de

† Present address: Department of Computational and Data Sciences and Computational Materials Science Center, George Mason University, 4400 University Drive, Fairfax, VA 22030

<sup>1</sup> K. Koepnik and H. Eschrig, *Full-potential nonorthogonal local-orbital minimum-basis band-structure scheme*, Phys. Rev. B **59**, 1743 (1999); <http://www.FPLO.de>

<sup>2</sup> J. P. Perdew, K. Burke, and M. Ernzerhof, *Generalized Gradient Approximation Made Simple*, Phys. Rev. Lett. **77**, 3865 (1996).

<sup>3</sup> G. Wang and X. Shi, *Electronic structures and magnetism of  $YM_2Ge_2$  ( $M = Mn-Cu$ ): Ge-height dependent magnetic ordering in  $YFe_2Ge_2$* , Comput. Mater. Sci. **121**, 48 (2016).

<sup>4</sup> A. Subedi, *Unconventional sign-changing superconductivity near quantum criticality in  $YFe_2Ge_2$* , Phys. Rev. B **89**, 024504 (2014).

<sup>5</sup> D. J. Singh, *Superconductivity and magnetism in  $YFe_2Ge_2$* , Phys. Rev. B **89**, 024505 (2014).

<sup>6</sup> I. I. Mazin and D. J. Singh, *Electronic structure and magnetism in Ru-based perovskites*, Phys. Rev. B **56**, 2556 (1997).